Gap solitons in a nonlinear quadratic negative-index cavity

Michael Scalora,[1] Domenico de Ceglia,[1,2] Giuseppe D'Aguanno,[1] Nadia Mattiucci,[1] Neset Akozbek,[3] Marco Centini,[4] and Mark J. Bloemer[1]

[1]*Charles M. Bowden Research Facility, AMSRD-AMR-WS-ST, US Army RDECOM, Redstone Arsenal, Alabama 35898, USA*

[2]*Dipartimento di Elettrotecnica ed Elettronica, Politecnico di Bari, Via Orabona 4, 70124 Bari, Italy*

[3]*Time Domain Corporation, Cummings Research Park 7057 Old Madison Pike, Huntsville, Alabama 35806, USA*

[4]*INFM at Dipartimento di Energetica, Universita di Roma "La Sapienza," Via A. Scarpa 16, 00161 Roma, Italy*

(Received 29 March 2006; revised manuscript received 6 March 2007; published 19 June 2007)

We predict the existence of gap solitons in a nonlinear, quadratic Fabry-Pérot negative index cavity. A peculiarity of a single negative index layer is that if magnetic and electric plasma frequencies are different it forms a photonic band structure similar to that of a multilayer stack composed of ordinary, positive index materials. This similarity also results in comparable field localization and enhancement properties that under appropriate conditions may be used to either dynamically shift the band edge, or for efficient energy conversion. We thus report that an intense, fundamental pump pulse is able to shift the band edge of a negative index cavity, and make it possible for a weak second harmonic pulse initially tuned inside the gap to be transmitted, giving rise to a gap soliton. The process is due to cascading, a well-known phenomenon that occurs far from phase matching conditions that limits energy conversion rates, it resembles a nonlinear third-order process, and causes pulse compression due to self-phase modulation. The symmetry of the equations of motion under the action of either an electric or a magnetic nonlinearity suggests that both nonlinear polarization and magnetization, or a combination of both, can lead to solitonlike pulses. More specifically, the antisymmetric localization properties of the electric and magnetic fields cause a nonlinear polarization to generate a dark soliton, while a nonlinear magnetization spawns a bright soliton.

DOI: 10.1103/PhysRevE.75.066606 PACS number(s): 42.65.Tg, 42.65.Ky, 42.70.Qs, 78.20.Ci

INTRODUCTION

The term "gap soliton" was coined to describe the shape that the electric field assumes when an incident, continuous wave beam is tuned inside the photonic band gap of a one-dimensional, periodic structure of finite length, so that a third order ($\chi^{(3)}$) nonlinearity causes the beam to be transmitted [1]. The physics of how such a state may be excited is exceptionally simple: A nonlinear change in the intensity-dependent refractive index of at least one of the constituent materials causes a shift of the photonic band edge, thus placing the incident beam within the pass band, and allowing its transmission. An excellent review of third order gap solitons may be found in Ref. [2]. Transverse, diffractive spatial gap solitons have been predicted in quadratic ($\chi^{(2)}$) materials in the context of multilayer structures [3], and are generally due to cascading, a process that occurs when pump and second harmonic beams interact far from phase matching conditions. Temporal, two-color gap solitons were also predicted in quadratic, shallow-depth Bragg gratings [4], and typically rely on doubly resonant conditions, and strong coupling between the fundamental (FF) and second harmonic (SH) beams. The recent interest in negative index materials (NIMs) [5] has led to predictions of $\chi^{(3)}$ gap solitons [6] near the band edge of the intrinsic gap of a Fabry-Pérot, NIM cavity [7] in the form of a single slab of material immersed in vacuum. Unlike the zero average-index gap [8], formation of the intrinsic band structure does *not* require the presence of a positive index material (PIM), and it is a peculiarity of the frequency range where a NIM has dielectric susceptibility and magnetic permeability of opposite signs [7]. The peculiarities of the band structure extend to the field localization properties, which appear to be unique even for a single slab of material [6,7].

In this paper we report second harmonic gap solitons in a $\chi^{(2)}$-active NIM cavity. For a positive nonlinear coefficient, one may excite either a dark or a bright soliton, depending on whether an electric or magnetic nonlinearity is present, and on the ratio of the magnetic and electric plasma frequencies. As is well known in the case of ordinary PIMs, the FF and SH fields do not exchange energy if the relative phase difference between the incident fields is chosen so that the interaction proceeds far from the phase matching condition, thus triggering cascading, and the interaction resembles a $\chi^{(3)}$ process. In a NIM cavity, the formation of a gap soliton at the second harmonic frequency follows a similar pattern, with some distinguishing characteristics. An intense, relatively narrow-bandwidth FF pulse is tuned to the first resonance peak (Fig. 1), on the low frequency side of the intrinsic band gap, where the index of refraction is negative, so that it resolves the resonance and it is mostly transmitted. This means that incident pump fields can become highly localized inside the NIM cavity, but the pulses can still propagate through the medium with minimal distortion and/or scattering losses and with near unit transmittance, as has been demonstrated near the band edge of a one-dimensional photonic band gap structure [9]. Although we choose the FF to be narrow-band and resonant, we note that these are not necessary conditions for the generation of solitonlike pulses, although this combination helps to lower the nonlinear thresholds [10,11]. A much weaker SH pulse is then tuned inside the gap (Fig. 1), where the index of refraction is near zero ($n \sim 10^{-3}$), in proximity of the high frequency band edge, so that in the absence of nonlinear coupling it is mostly reflected. In general, the SH pulse tends to gain energy.

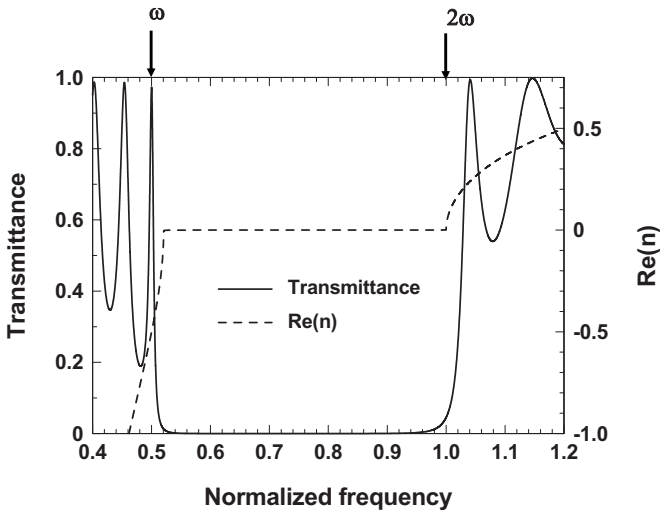

FIG. 1. Transmittance (left axis) and real part of the index of refraction (right axis) for the Drude model described in the text, with $\tilde{\omega}_M=1$, $\tilde{\omega}_E=0.5205$, and $\tilde{\Gamma}=10^{-4}$. The FF pulse is tuned at $\omega=0.5$, which coincides with the first band edge resonance on the low frequency side. The SH pulse is tuned to $\omega=1$, which falls inside the gap.

However, by adjusting the relative input phase difference between the fields a condition exists such that the SH pulse experiences no net gain, causing instead a dynamic shift of the band edge. As a result, the SH pulse is effectively pushed out of the band gap, it is spatially and temporally compressed by self-phase modulation, and almost completely transmitted: Transmittance switches from 4% to about 90%.

PROPAGATION MODEL

To model the dynamics of interacting, short FF and SH pulses in a dispersive material one can choose from a number of available approaches. For simplicity, we assume one-dimensional nonlinear pulse propagation, and follow the development of optical harmonic generation found in Boyd [12]. One may assume that the material contains a fine scale structure that gives rise to a second order nonlinearity, which is then uniformly distributed inside the material. Then, if the fields are linearly polarized, they may be expressed as a superposition of fundamental and higher harmonic frequencies as follows [12]:

$$\mathbf{E}=\hat{\mathbf{x}}\sum_{\ell=1}^{\infty}[E_{\ell\omega}(z,t)+\text{c.c.}]=\hat{\mathbf{x}}\sum_{\ell=1}^{\infty}[\mathcal{E}_{\ell\omega}(z,t)e^{i\ell(k_0z-\omega_0t)}+\text{c.c.}],$$

$$\mathbf{H}=\hat{\mathbf{y}}\sum_{\ell=1}^{\infty}[H_{\ell\omega}(z,t)+\text{c.c.}]=\hat{\mathbf{y}}\sum_{\ell=1}^{\infty}[\mathcal{H}_{\ell\omega}(z,t)e^{i\ell(k_0z-\omega_0t)}+\text{c.c.}], \tag{1}$$

where ℓ is a positive integer that denotes the ℓth harmonic. In Eqs. (1), each harmonic is expressed as the product of a generic envelope function and oscillating factors that contain carrier wave vector and frequency. $k_0=\omega_0/c$ is the free space wave vector, and ω_0 is the corresponding carrier pump frequency. The pump pulses are assumed to be initially located in free space, and no assumptions are made about the envelope functions. The nonlinear polarization and magnetization that evolve inside the medium may also be described in a manner similar to Eqs. (1), each in terms of a generic envelope function and carrier wave vector and frequency as follows:

$$\mathbf{P}_{\text{NL}}=\hat{\mathbf{x}}\sum_{\ell=1}^{\infty}[\mathcal{P}_{\ell\omega}(z,t)e^{i\ell(k_0z-\omega_0t)}+\text{c.c.}],$$

$$\mathbf{M}_{\text{NL}}=\hat{\mathbf{y}}\sum_{\ell=1}^{\infty}[\mathcal{M}_{\ell\omega}(z,t)e^{i\ell(k_0z-\omega_0t)}+\text{c.c.}]. \tag{2}$$

For the kind of simplified second order nonlinear process we are considering, it suffices to assume nonlinear polarization and magnetization of the type $P_{\text{NL}}=\chi_P^{(2)}E^2$, and $M_{\text{NL}}=\chi_M^{(2)}H^2$, where $\chi_P^{(2)}$ and $\chi_M^{(2)}$ are the respective electric and magnetic nonlinear coefficients, which in turn are also allowed to be arbitrary functions of position, i.e., they may be discontinuous along the longitudinal coordinate. The nonlinear polarization and magnetization in Eqs. (2) can then be easily expanded. For example, retaining terms up to the fourth harmonic frequency, the corresponding nonlinear polarization terms become [12]

$$\mathcal{P}_{\omega}(z,t)=2\chi_P^{(2)}(\mathcal{E}_{\omega}^{*}\mathcal{E}_{2\omega}+\mathcal{E}_{2\omega}^{*}\mathcal{E}_{3\omega}+\mathcal{E}_{3\omega}^{*}\mathcal{E}_{4\omega}+\cdots),$$

$$\mathcal{P}_{2\omega}(z,t)=\chi_P^{(2)}(\mathcal{E}_{\omega}^{2}+2\mathcal{E}_{\omega}^{*}\mathcal{E}_{3\omega}+2\mathcal{E}_{2\omega}^{*}\mathcal{E}_{4\omega}+\cdots),$$

$$\mathcal{P}_{3\omega}(z,t)=2\chi_P^{(2)}(\mathcal{E}_{\omega}\mathcal{E}_{2\omega}+\mathcal{E}_{\omega}^{*}\mathcal{E}_{4\omega}+\cdots),$$

$$\mathcal{P}_{4\omega}(z,t)=\chi_P^{(2)}(\mathcal{E}_{2\omega}^{2}+2\mathcal{E}_{\omega}\mathcal{E}_{3\omega}+\cdots). \tag{3}$$

The nonlinear magnetization terms have a similar form. Although we have omitted fifth and higher harmonics from the expansion, they may be found without difficulty.

The model that we adopt takes linear, background material dispersion (including absorption) into account. Following Eqs. (2), the displacement field **D** may be similarly defined as follows:

$$\mathbf{D}=\hat{\mathbf{x}}\sum_{t=1}^{\infty}[D_{\ell\omega}(z,t)+\text{c.c.}]=\hat{\mathbf{x}}\sum_{\ell=1}^{\infty}[\mathcal{D}_{\ell\omega}(z,t)e^{i\ell(k_0z-\omega_0t)}+\text{c.c.}], \tag{4}$$

which may be related to the electric field by expanding the complex dielectric function as a Taylor series in the usual way:

$$\varepsilon(z,\omega)=\varepsilon(z,\omega_0)+\left.\frac{\partial\varepsilon(z,\omega)}{\partial\omega}\right|_{\omega_0}(\omega-\omega_0)+\frac{1}{2}\left.\frac{\partial^2\varepsilon(z,\omega)}{\partial\omega^2}\right|_{\omega_0}(\omega-\omega_0)^2+\cdots$$
$$=a(z,\omega_0)+b(z,\omega_0)\omega+c(z,\omega_0)\omega^2+\cdots. \tag{5}$$

For an isotropic background medium, a simple constitutive

relation may be written to relate each harmonic to its relative displacement field. It is then easy to show that, in general [13–18],

$$\frac{\partial D_{\ell\omega}(z,t)}{\partial t} = \left\{ -i\omega_0 \varepsilon_{\ell\omega}(\omega_0)\mathcal{E}_{\ell\omega} + \left[\frac{\partial[\omega\varepsilon_{\ell\omega}(\omega)]}{\partial\omega}\right]_{\omega_0} \frac{\partial \mathcal{E}_{\ell\omega}}{\partial t} + \frac{i}{2}\left[\frac{\partial^2[\omega\varepsilon_{\ell\omega}(\omega)]}{\partial\omega^2}\right]_{\omega_0} \frac{\partial^2 \mathcal{E}_{\ell\omega}}{\partial t^2} + \cdots \right\} e^{-i\ell\omega_0 t}. \tag{6}$$

In addition to directly entering Maxwell's equations, Eq. (6) is also important for the purpose of determining electromagnetic energy density and losses when material dispersion is present [13], and when pulses are especially short. Therefore, assuming a nonzero $\chi^{(2)}$, the scaled Maxwell's equations for the ℓth harmonic take the following form [14–18]:

$$\alpha_{\ell\tilde{\omega}}\frac{\partial \mathcal{E}_{\ell\tilde{\omega}}}{\partial\tau} + i\frac{\alpha'_{\ell\tilde{\omega}}}{4\pi}\frac{\partial^2 \mathcal{E}_{\ell\tilde{\omega}}}{\partial\tau^2} - \frac{\alpha''_{\ell\tilde{\omega}}}{24\pi^2}\frac{\partial^3 \mathcal{E}_{\ell\tilde{\omega}}}{\partial\tau^3} + \cdots = i\ell\beta(\varepsilon_{\ell\tilde{\omega},\xi}\mathcal{E}_{\ell\tilde{\omega}} - \mathcal{H}_{\ell\tilde{\omega}}) - \frac{\partial \mathcal{H}_{\ell\tilde{\omega}}}{\partial\xi} + 4\pi\left(i\ell\beta\mathcal{P}_{\ell\tilde{\omega}} - \frac{\partial \mathcal{P}_{\ell\tilde{\omega}}}{\partial\tau}\right),$$

$$\gamma_{\ell\tilde{\omega}}\frac{\partial \mathcal{H}_{\ell\tilde{\omega}}}{\partial\tau} + i\frac{\gamma'_{\ell\tilde{\omega}}}{4\pi}\frac{\partial^2 \mathcal{H}_{\ell\tilde{\omega}}}{\partial\tau^2} - \frac{\gamma''_{\ell\tilde{\omega}}}{24\pi^2}\frac{\partial^3 \mathcal{H}_{\ell\tilde{\omega}}}{\partial\tau^3} + \cdots = i\ell\beta(\mu_{\ell\tilde{\omega},\xi}\mathcal{H}_{\ell\tilde{\omega}} - \mathcal{E}_{\ell\tilde{\omega}}) - \frac{\partial \mathcal{E}_{\ell\tilde{\omega}}}{\partial\xi} + 4\pi\left(i\ell\beta\mathcal{M}_{\ell\tilde{\omega}} - \frac{\partial \mathcal{M}_{\ell\tilde{\omega}}}{\partial\tau}\right), \tag{7}$$

where $\alpha_{\ell\tilde{\omega}} = (\partial[\tilde{\omega}\varepsilon_{\ell\tilde{\omega}}(\xi)]/\partial\tilde{\omega})|_{\omega_0}$, $\gamma_{\ell\tilde{\omega}} = (\partial[\tilde{\omega}\mu_{\ell\tilde{\omega}}(\xi)]/\partial\tilde{\omega})|_{\omega_0}$, and the prime symbol denotes a derivative with respect to frequency; together with $\varepsilon_{\ell\tilde{\omega}}$ and $\mu_{\ell\tilde{\omega}}$, $\alpha_{\ell\tilde{\omega}}$ and $\gamma_{\ell\tilde{\omega}}$ are also complex functions of frequency and of the spatial coordinate. We have chosen $\lambda_0 = 1$ μm as the reference wavelength, and have adopted the following scaling: $\xi = z/\lambda_0$ is the scaled longitudinal coordinate; $\tau = ct/\lambda_0$ is the time in units of the optical cycle; $\beta = 2\pi\tilde{\omega}$ is the scaled wave vector; $\tilde{\omega} = \omega/\omega_0$ is the scaled frequency, and $\omega_0 = 2\pi c/\lambda_0$, where c is the speed of light in vacuum. The cavity is assumed to be two microns in length, and its transmission function is shown is Fig. 1.

At this point, for pedagogical purposes it is worthwhile to digress and discuss some of the details regarding the method of solution, the assumptions and approximations that are made to solve Eqs. (7), and to give additional related background information abut the model. In deriving Eqs. (7), we have assumed that the background medium is isotropic, and that pulses do not diffract. The latter restriction simply means that transverse beam width remains many wavelengths wide at all times. This limitation can easily be lifted by allowing the fields to vary along the transverse coordinate [16]. More importantly, our description of the fields as the product of an envelope function and a carrier wave vector and frequency is a mere matter of convenience, primarily because it allows one to follow the detailed dynamics of each harmonic, and to explore the impact of each term on the dynamics. However, it should be noted that although this field decomposition constitutes the foundation of the slowly varying envelope approximation, it should not *per se* be misconstrued as an approximation, because Eqs. (7) do not contain any restrictions on the envelope functions. While in principle the number of linear dispersion terms (temporal derivatives of the fields) and/or the number of harmonics one retains to describe the system may be arbitrarily large, in practice one must work with a finite number of them. Of course, truncating the number of time derivatives or the number of harmonics is equivalent to making some kind of approximation.

In the system that we consider, which entails input FF and SH pulses, and a medium only a few wavelengths thick, it is more than sufficient to neglect third and higher harmonics, and to neglect second and higher temporal derivatives that arise from linear material dispersion [10,11,14–18]. We can be more specific and quantify each of these aspects separately. For instance, retention of third and fourth harmonic fields in Eqs. (7) leads to third and fourth harmonic conversion rates of $\sim 10^{-7}$ and $\sim 10^{-9}$, respectively. Therefore, it is clear that the calculations may be simplified by truncating nonlinear polarization and magnetization terms at the second harmonic fields without appreciably impacting the dynamics. In terms of linear material dispersion, propagation distances that typically do not exceed a few tens of wavelengths also make it possible to neglect second and higher order temporal derivatives, *without* the need to perform a slowly varying envelope approximation in time [10,11,19]. That is to say, it can easily be demonstrated that if the medium is only a few tens of wavelengths thick, as is always the case in nano- and micron-sized structures, the dielectric constant of Eq. (5) can be accurately represented by the first two leading terms, even if a pulse were only a few optical cycles in duration. Of course, the truncation of Eq. (5) at the second term becomes a material characterization, not an approximation imposed on the envelope function.

These notions have been theoretically analyzed in depth and verified in the case of ultrashort pulse propagation in a number of scenarios that comprise real materials, including metallodielectric, multilayer stacks [16], and negative index materials [14,16–18]. Some practical examples should help clarify the nature of this approximation. In the case of a typical metallodielectric nanostructure composed of noble metals and dispersive dielectric materials such as Si_3N_4 or GaAs, for example, in the visible range one typically finds that $|\alpha_\omega \dot{\mathcal{E}}_\omega|/(|\alpha'_\omega \ddot{\mathcal{E}}_\omega|/4\pi) \sim 40$ for a two-optical cycle pulse [17], with even larger ratios for higher harmonics. As another example, in a negative index material second order dispersion lengths may easily approach several hundred wavelengths even for pulses only a few optical cycles in duration [20]. Therefore, under most circumstances of interest that involve pulse propagation in relatively thin media, Eqs. (7) may safely and accurately be recast as follows [18]:

$$\alpha_{\ell\tilde{\omega}}\frac{\partial \mathcal{E}_{\ell\tilde{\omega}}}{\partial \tau} \approx i\ell\beta(\varepsilon_{\ell\tilde{\omega},\xi}\mathcal{E}_{\ell\tilde{\omega}} - \mathcal{H}_{\ell\tilde{\omega}}) - \frac{\partial \mathcal{H}_{\ell\tilde{\omega}}}{\partial \xi} + 4\pi\left(i\ell\beta\mathcal{P}_{\ell\tilde{\omega}} - \frac{\partial \mathcal{P}_{\ell\tilde{\omega}}}{\partial \tau}\right),$$

$$\gamma_{\ell\tilde{\omega}}\frac{\partial \mathcal{H}_{\ell\tilde{\omega}}}{\partial \tau} \approx i\ell\beta(\mu_{\ell\tilde{\omega},\xi}\mathcal{H}_{\ell\tilde{\omega}} - \mathcal{E}_{\ell\tilde{\omega}}) - \frac{\partial \mathcal{E}_{\ell\tilde{\omega}}}{\partial \xi} + 4\pi\left(i\ell\beta\mathcal{M}_{\ell\tilde{\omega}} - \frac{\partial \mathcal{M}_{\ell\tilde{\omega}}}{\partial \tau}\right). \quad (8)$$

In summary, in addition to the assumptions that the background medium is isotropic and diffraction is neglected, the final Eqs. (8) for the ℓth harmonic contain the following simplifications: (i) Second and higher-order, linear material dispersion terms are neglected; (ii) third and higher harmonics are also neglected. As written, Eqs. (8) provide an accurate physical picture of the dynamics, including boundary conditions and all orders of reflections, even for pulses that are just a few wave cycles in duration.

To make sure that the approximations and assumptions discussed in the previous paragraphs are indeed valid, we also integrated Maxwell's equations using a finite difference, time domain algorithm similar to the one discussed in Ref. [21]. We then compared the solutions of Eqs. (8) to the solutions of the following set of equations [22]:

$$\frac{\partial E_x}{\partial t} = -\frac{1}{\varepsilon_0}\left[\frac{\partial H_y}{\partial z} + J_x\right] - \chi_e^{(2)}\frac{\partial E_x^2}{\partial t}, \quad \frac{\partial J_x}{\partial t} + \Gamma_e J_x = \varepsilon_0\omega_e^2 E_x,$$

$$\frac{\partial E_y}{\partial t} = -\frac{1}{\mu_0}\left[\frac{\partial E_x}{\partial z} + K_y\right] - \chi_m^{(2)}\frac{\partial H_y^2}{\partial t}, \quad \frac{\partial K_y}{\partial t} + \Gamma_m K_y = \mu_0\omega_m^2 H_y. \quad (9)$$

In Eq. (9), J_x and K_y are the electric and magnetic current densities, respectively, and $\Gamma_{e,m}$ are the corresponding damping coefficients. The integration of Eqs. (8) and (9) are carried out for pulses whose durations varied from a few optical cycles up to several picoseconds, with indistinguishable results in all cases investigated. In addition to having more control over each term, Maxwell's Eqs. (8) are written in a form that allows the use of the classic fast Fourier transform, beam propagation method [23], appropriately modified to include all orders of reflections and feedback in the time domain [19]. We use a spectral method primarily because it involves multiplication of linear operators; it is unconditionally stable, with no known issues relating to phase or amplitude errors, and thus not prone to the generation of any numerical artifacts; and it can easily be extended to the multidimensional domain almost effortlessly [16,17].

$\chi^{(2)}$ GAP SOLITONS

The intrinsic band gap, the relative tuning of the FF and SH fields, and the index of refraction are depicted in Fig. 1, given a Drude model with the following characteristics: $\varepsilon(\tilde{\omega}) = 1 - \tilde{\omega}_E^2/(\tilde{\omega}^2 + i\tilde{\Gamma}\tilde{\omega})$, $\mu(\tilde{\omega}) = 1 - \tilde{\omega}_M^2/(\tilde{\omega}^2 + i\tilde{\Gamma}\tilde{\omega})$, where $\tilde{\omega}_E = \omega_E/\omega_0$ and $\tilde{\omega}_M = \omega_M/\omega_0$ are the scaled electric and magnetic plasma frequencies, respectively, and $\tilde{\Gamma}$ is the scaled damping coefficient. As a representative example, we choose $\tilde{\omega}_M = 1$, $\tilde{\omega}_E = 0.5205$, and $\tilde{\Gamma} = 10^{-4}$. Therefore, the *magnetic* plasma frequency coincides with our reference wavelength. Although it is never explicitly invoked in the integrations of Maxwell's equations, the index of refraction may be retrieved as usual, i.e., $n(\tilde{\omega}) = \pm\sqrt{\varepsilon(\tilde{\omega})\mu(\tilde{\omega})}$, and the negative root is chosen when both ε and μ are simultaneously negative [5]. Our choice of $\tilde{\Gamma}$ corresponds to an absorption length of approximately 500 microns for the pump, and ten times larger for the SH pulse, so that neither are appreciably attenuated, as the transmittance curve of Fig. 1 shows. However, our calculations suggest that the soliton does not loose its coherence with the introduction of more significant absorption, whose presence tends to simply raise the nonlinear thresholds. For example, taking $\tilde{\Gamma} = 10^{-3}$, which corresponds to an absorption length of ~ 50 μm, causes the transmittance of the FF to drop to $\sim 77\%$. Our calculations show that this loss may be compensated by a $\sim 30\%$ increase in the peak intensity of the FF pulse. In sum, the resulting dynamics is relatively stable against tuning with respect to the band edge, and the introduction of absorption.

Unlike the damping coefficient, $\tilde{\omega}_M$ and $\tilde{\omega}_E$ contain more subtleties, primarily because their relative magnitudes determine how the fields will become localized [7]. We note that experimentally, $\tilde{\omega}_M$ and $\tilde{\omega}_E$ may be set by properly engineering the size of the elemental, split-ring resonator circuit [24], or by properly managing the geometry of the various components [25]. Then, our initial choice of smaller electric plasma frequency causes the electric field to become highly localized (a single maximum) at the low frequency band edge, and antilocalized (a single minimum) at the high frequency band edge, near the second harmonic frequency. Exchanging the values of $\tilde{\omega}_M$ and $\tilde{\omega}_E$ causes the electric and magnetic fields to trade roles, as an analysis of Eqs. (7) or (8) suggests. Consequently, the nonlinear polarization generates antilocalized, dark gap solitons when $\tilde{\omega}_E < \tilde{\omega}_M$, and a nonlinear magnetization induces localized, bright gap solitons if the situation is reversed, namely when $\tilde{\omega}_M < \tilde{\omega}_E$. In Fig. 2 we show the antilocalized and localized states that respectively correspond to the excitation of dark and bright solitons, for a SH frequency tuned near the high frequency band edge resonance. In Fig. 3 we depict the energy contained in the SH pulse as a function of the relative input phase difference between the two incident pulses, normalized in units of the incident, SH energy. When $\delta\varphi \sim 10.5°$, the energy exchanged between the fields amounts to less than one part in a thousand. The temporal dynamics of the integrated SH energy is shown in Fig. 4. Each point on the curves of Fig. 3 was obtained using incident pulses approximately 1.5 ps in duration, or about 200 optical cycles at the reference wavelength of 1 μm; the intensity of the FF (~ 100 MW/cm^2) is approximately 2×10^5 greater than the SH peak intensity, so that the FF field propagates undisturbed; and $\chi_P^{(2)} \sim 8$ pm/V and $\chi_M^{(2)} = 0$. In Fig. 5 we show incident and scattered SH pulse intensities, normalized to incident peak intensity. The figure reveals that in addition to being mostly transmitted,

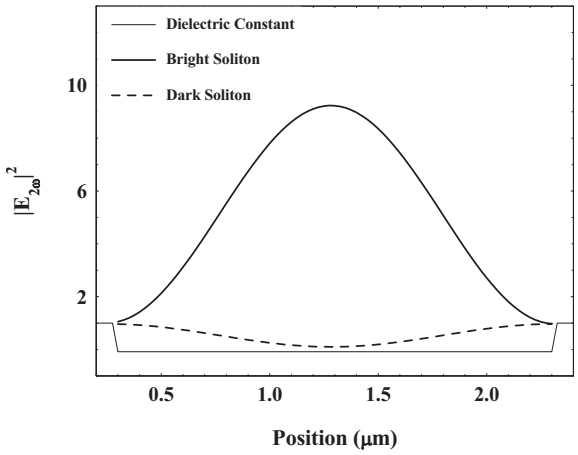

FIG. 2. Dashed curve: Dark SH soliton. This state is excited by the pump field interacting with a nonlinear polarization, as the band edge dynamically shifts and tunes the SH frequency near the first high frequency band edge resonance. The bright, SH soliton (thick, solid curve) is excited via a nonlinear magnetization, and by swapping the values of $\tilde{\omega}_M$ and $\tilde{\omega}_E$ cited in the caption of Fig. 1, such that $\tilde{\omega}_E=1$, $\tilde{\omega}_M=0.5205$. The thin, solid line traces the real part of the dielectric function.

the pulse is compressed by ~30%. One should contrast these results with linear behavior, i.e., Fig. 1, where we obtain ~4% transmission. The group velocity of the transmitted pulse is estimated at $\sim c/18$. All these aspects of the dynamics, i.e., high transmittance, pulse compression, and the significant reduction of group velocity, are fully consistent with solitonlike behavior near the photonic band edge, as observed experimentally in the case of a soliton that forms and propagates near the band edge of a fiber Bragg grating [26]. In Ref. [26], a 60 ps (spatial extension ~20 millimeters) was narrowed by nearly 50% as a result self-phase modulation that occurred near the band edge of a nonlinear Bragg grating 55 millimeters in length. The length of the grating was chosen to allow nonlinear effects to develop in an environment

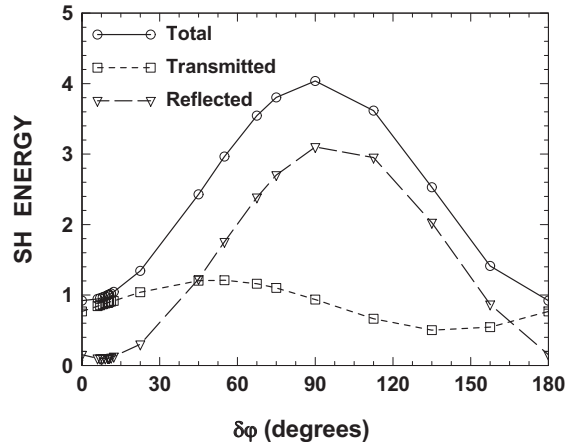

FIG. 3. Integrated SH energy as a function of relative phase difference between incident FF and SH pulses, normalized with respect to incident SH energy. A total energy value near unity thus corresponds to a point of no net energy exchange between the fields, and to maximum dynamics shift of the band edge.

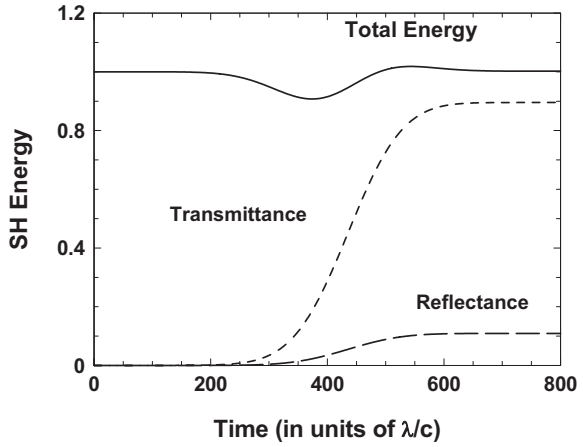

FIG. 4. Temporal dynamics of the total, transmitted (to the right of the structure in Fig. 4), and reflected (to the left of the structure in Fig. 4) SH energies for $\delta\varphi\sim 10.5°$. Transient behavior is evident in the total, instantaneous energy. The overall transmission settles to approximately 90%. The generic incident field envelops are of the type $\mathcal{E}_\omega, \mathcal{H}_\omega(\xi,0)=\mathcal{E}_0^{(\omega)}$, $\mathcal{H}_0^{(\omega)}e^{-(\xi-\xi_0)^2/w^2}e^{i\varphi}$ for the fundamental, and $\mathcal{E}_{2\omega}, \mathcal{H}_{2\omega}(\xi,0)=\mathcal{E}_0^{(2\omega)}$, $\mathcal{H}_0^{(2\omega)}e^{-(\xi-\xi_0)^2/w^2}$ for the second harmonic fields. In our units, the choice of $w\sim 200$ corresponds to a pulse with full width at half maximum of ~1.5 ps.

having shallow linear index modulation ($\delta n\sim 10^{-4}$). In our case, just as it occurs in photonic band gap structures of finite length having deep gratings, typical nonlinear lengths are just a few microns thanks to the much larger degree of field confinement and density of modes compared to shallow gratings [27]. However, the dynamics follows similar patterns in both cases.

CONCLUSIONS

The dynamics that we have described depend on a number of factors. For instance, the curves of Fig. 3 are sensitive

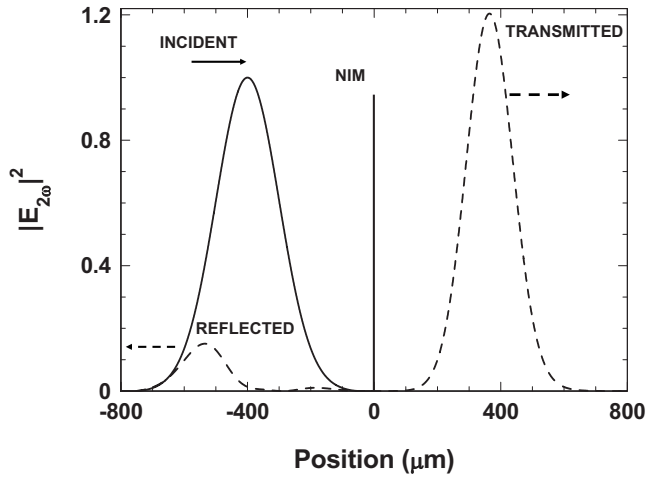

FIG. 5. Incident and scattered SH pulses. The figure shows that the peak intensity of the transmitted pulse increases by approximately 20%, and its full width at half maximum decreases by approximately 30%. The group velocity of the transmitted pulse is calculated to be $\sim c/18$.

not only to initial relative phase difference, but also to peak pulse intensities. Because of this sensitivity, pulse duration is also important, as pulse bandwidth determines the degree of localization light achieves inside the etalon. In our analysis we have used narrow-bandwidth pulses that resolve well the band edge resonance, and lead to maximum field localization inside the cavity. Thus the kind of gap soliton that we report persists well into the subpicosecond regime, and as we have seen, it is resistant to absorption and tuning with respect to the band edge, albeit with relatively higher nonlinear thresholds.

In summary, we report SH bright and dark gap solitons in a relatively high-Q, 2 μm thick, nonlinearly Fabry-Pérot cavity. The relative phase difference between the incident fields is chosen to induce cascading processes and a dynamic shift of the intrinsic band edge that causes pulse compression and gap soliton formation. The soliton is relatively impervious to the introduction of absorption, tuning with respect to the band edge, and the reduction of pulse width. These findings are relevant in the optical regime, as negative index materials are actually being fabricated in the near IR region [25], with good prospects for devices in the visible part of the spectrum. We thus hope that our results, which take into account effects of finite size and material absorption, will further stimulate research in this direction. Finally, we note that gap solitons at the fundamental frequency may also be created using a negative nonlinear coefficient, and by reversing the roles and intensities of the SH and FF pulses.

ACKNOWLEDGMENTS

G.D. and N.M. thank the National Research Council for financial support. D.d.C. thanks the US Army European Research Office for partial financial support.

[1] W. Chen and D. L. Mills, Phys. Rev. Lett. **58**, 160 (1987).
[2] C. M. de Sterke and J. E. Sipe, in *Progress in Optics XXXIII*, edited by E. Wolf (Elsevier, Amsterdam, 1994), Chap. 3, and references therein.
[3] Y. S. Kivshar, Phys. Rev. E **51**, 1613 (1995).
[4] C. Conti, S. Trillo, and G. Assanto, Phys. Rev. Lett. **78**, 2341 (1997).
[5] V. G. Veselago, Sov. Phys. Usp. **10**, 509 (1968); Opt. Express **11**, pp. 639–760 (2003), focus issue on negative refraction and metamaterials; J. Opt. Soc. Am. B **23**, pp. 386–583 (2006), focus issue on metamaterials.
[6] G. D'Aguanno, N. Mattiucci, M. Scalora, and M. J. Bloemer, Phys. Rev. Lett. **93**, 213902 (2004).
[7] G. D'Aguanno, N. Mattiucci, M. Scalora, and M. J. Bloemer, Laser Phys. **15**, 590 (2005).
[8] J. Li, L. Zhou, C. T. Chan, and P. Sheng, Phys. Rev. Lett. **90**, 083901 (2003).
[9] M. Scalora, R. J. Flynn, S. B. Reinhardt, R. L. Fork, M. J. Bloemer, M. D. Tocci, C. M. Bowden, H. S. Ledbetter, J. M. Bendickson, J. P. Dowling, and R. P. Leavitt, Phys. Rev. E **54**, R1078 (1996).
[10] M. Scalora, M. J. Bloemer, A. S. Manka, J. P. Dowling, C. M. Bowden, R. Viswanathan, and J. W. Haus, Phys. Rev. A **56**, 3166 (1997).
[11] R. W. Boyd, *Nonlinear Optics*, 2nd ed. (Academic Press, San Diego, 2003).
[12] M. Centini, G. D'Aguanno, M. Scalora, C. Sibilia, M. Bertolotti, M. J. Bloemer, and C. M. Bowden, Phys. Rev. E **64**, 046606 (2001).
[13] L. D. Landau and E. M. Lifshitz, *Electrodynamics of continuous media* (Pergamon Press, New York, 1960), pp. 253–256.
[14] M. Scalora, G. D'Aguanno, N. Mattiucci, N. Akozbek, M. J. Bloemer, M. Centini, C. Sibilia, and M. Bertolotti, Phys. Rev. E **72**, 066601 (2005).
[15] M. Scalora, M. S. Syrchin, N. Akozbek, E. Y. Poliakov, G. D'Aguanno, N. Mattiucci, M. J. Bloemer, and A. M. Zheltikov, Phys. Rev. Lett. **95**, 013902 (2005).
[16] M. Scalora, G. D'Aguanno, N. Mattiucci, M. J. Bloemer, J. W. Haus, and A. M. Zheltikov, Appl. Phys. B: Lasers Opt. **81**, 393 (2005).
[17] M. Scalora, N. Mattiucci, G. D'Aguanno, M. C. Larciprete, and M. J. Bloemer, Phys. Rev. E **73**, 016603 (2006).
[18] M. Scalora, G. D'Aguanno, M. J. Bloemer, M. Centini, D. de Ceglia, N. Mattiucci, and Y. S. Kivshar, Opt. Express **14**, 4746 (2006).
[19] M. Scalora and M. E. Crenshaw, Opt. Commun. **108**, 191 (1994); M. Scalora, in *Nanoscale Linear and Nonlinear Optics*, edited by Bertolotti, Bowden, and Sibilia, AIP Conf. Proc. No. 560 (AIP, Melville, NY, 2001), p. 298.
[20] G. D'Aguanno, N. Akozbek, N. Mattiucci, M. Scalora, M. J. Bloemer, and A. M. Zheltikov, Opt. Lett. **30**, 1998 (2005).
[21] R. W. Ziolkowski and E. Heyman, Phys. Rev. E **64**, 056625 (2001).
[22] D. de Ceglia, A. D'Orazio, M. DeSario, V. Petruzzelli, F. Prudenzano, M. Centini, M. G. Cappeddu, M. J. Bloemer, and M. Scalora, Opt. Lett. **32**, 3 (2007)
[23] M. D. Feith and J. A. Fleck, Jr., Appl. Opt. **17**, 3990 (1978); **19**, 2240 (1980).
[24] R. A. Shelby, D. R. Smith, and S. Schultz, Science **292**, 77 (2001); C. G. Parazzoli *et al.*, Phys. Rev. Lett. **90**, 107401 (2003).
[25] V. M. Shalaev, W. Cai, U. K. Chettiar, H.-K. Yuan, A. K. Sarychev, V. P. Drachev, and A. V. Kildishev, Opt. Lett. **30**, 3356 (2005).
[26] B. J. Eggleton, R. E. Slusher, C. M. de Sterke, P. A. Krug, and J. E. Sipe, Phys. Rev. Lett. **76**, 1627 (1996).
[27] M. Scalora, J. P. Dowling, M. J. Bloemer, and C. M. Bowden, Phys. Rev. Lett. **73**, 1368 (1994).